16th World Conference on Earthquake, 16WCEE 2017

Santiago Chile, January 9th to 13th 2017

Paper N° 277

Registration Code: S-B1462980033

SEISMIC RISK ASSESSMENT OF LIFELINES IN NEAR-FAULT AREAS

F. Cavalieri[1], P. Franchin[2], F. Mollaioli[3]

[1] *Research Associate, Sapienza University of Rome, Dept. Structural & Geotechnical Engineering, francesco.cavalieri@uniroma1.it*
[2] *Associate Professor, Sapienza University of Rome, Dept. Structural & Geotechnical Engineering, paolo.franchin@uniroma1.it*
[3] *Associate Professor, Sapienza University of Rome, Dept. Structural & Geotechnical Engineering, fabrizio.mollaioli@uniroma1.it*

Abstract

In proximity of a seismogenic source (*near-fault* or *near-source*), meaning for maximum distances ranging from about one km to a few tens of km as a function of earthquake magnitude, the ground motion produced by strong earthquakes presents typical characteristics in terms of amplitude, duration and frequency content, and it may be characterised by the *forward-directivity* (FD), *neutral-directivity* (ND) or *backward-directivity* (BD) phenomena. As a consequence of such directivity phenomena, for the case of forward-directivity the velocity waveform includes one or two pulses, typically of long duration, producing significant motion amplification for the sites in the direction of rupture propagation, while for the case of backward-directivity it includes a long duration and lower amplitude motion for the sites in the opposite direction. Any element at risk located in a region close to an active fault may also be subjected to a permanent static displacement due to fault slip, namely *fling step*. These characteristics may significantly affect the seismic response of structures in nonlinear field, and in general the extent and distribution of damage on urban infrastructural systems (such as buildings, lifelines, critical facilities).

This paper aims to estimate the role played by near-fault motions in the seismic risk assessment of lifelines composed of buried pipelines, such as water supply systems (WSS). The employed methodology involves four levels: seismic hazard, seismic fragility of components, systemic performance and uncertainty. First, several near-fault seismic records, characterized by the presence of an evident velocity pulse, are selected in order to highlight and take into account the FD effects; in particular, the pulses extracted from the records are used to obtain the probability distribution of a novel modification factor for Peak Ground Velocity (PGV), computed by an existing ground motion prediction equation. Also, a fling step model is selected from the ones currently available in the literature. Successively, the seismic demand is applied to the components of infrastructural systems by means of fragility or vulnerability functions, accounting for the uncertainty related to the physical damage state as a function of local seismic intensity. Then, a number of performance metrics are introduced to quantitatively measure the performance of a single system or the whole infrastructure (considering the interdependencies between systems). Two Monte Carlo simulations, in which the near-source effects are neglected and considered, respectively, are then employed to carry out a probabilistic analysis including the treatment of several uncertainties in the problem (in both hazard and system parts). The comparison of results from the two simulations allows to assess the importance of including near-source phenomena in seismic risk assessments.

The methodology was implemented as an extension of a civil infrastructure simulation tool, namely Object-Oriented Framework for Infrastructure Modeling and Simulation (OOFIMS), coded in MATLAB® language and recently developed in the SYNER-G (2012) European project. The tool was used to carry out an example application on a realistic WSS.

The findings of this study are of use for emergency managers and lifeline asset managers in tectonically-active urban settings, in order to increase the seismic resilience of communities.

Keywords: Pulse extraction; Fling step; Infrastructure; Buried pipelines; Monte Carlo simulation

1. Introduction

The ground motion produced by strong earthquakes in proximity of a seismogenic source (*near-fault* or *near-source*), i.e. for maximum distances ranging from about one km to a few tens of km as a function of earthquake magnitude, presents typical characteristics in terms of amplitude, duration and frequency content. As a consequence, such a motion may significantly affect the seismic response of structures in nonlinear field, and in general the extent and distribution of damage on urban *infrastructures*.

An infrastructure can be seen as a network of systems and processes that function collaboratively and synergistically to produce and distribute a continuous flow of essential goods and services (PCCIP, 1997). From a system-theoretic point of view, the infrastructure is a system of systems (SOS) (Rinaldi, 2004), including a number of systems (buildings, lifelines, critical facilities, etc.) whose reliable operation is essential to safety, health and all socio-economic activities of modern societies. This is the reason why it is commonly termed Critical Infrastructure (CI) (PCCIP, 1997).

The description of the near-fault seismic motion has raised in the last decade a growing interest in the Earthquake Engineering community, not only for the observed effects due to recent earthquakes, but also for the implications in modern seismic codes. It has been recognized that the motion results mainly influenced by the seismogenic characteristics of the source, the mechanism (normal, reverse, strike-slip faulting), the rupture evolution and the site position with respect to the maximum energy release zone. The propagation of fault rupture toward a near-source site with a velocity that is slightly less than that of shear waves causes most of the rupture seismic energy to accumulate in a large pulse, which can be noted at the beginning of the record (Somerville et al., 1997). Such effect, being typically long period, is more evident in the velocity and displacement time histories than in the acceleration one. Based on the fault geometry and the direction of rupture propagation, this large pulse is oriented along the direction perpendicular to the fault and is characterized by a fault-normal (FN) component that is stronger than the fault-parallel (FP) one. Any element at risk located in a region close to an active fault may also be subjected to a significant permanent static displacement due to fault slip, namely *fling step*.

Current literature features several attempts (e.g., Baker, 2007) to include near-source effects in existing ground motion prediction equation (GMPE) models, for applications to structures. Among the different systems that can compose an urban infrastructure (point-like, line-like, area-like systems), the focus in this study is on spatially distributed systems, and in particular the lifelines composed of buried pipelines: examples are given by water supply systems (WSS), storm water networks (SWN), wastewater networks (WWN) and gas distribution networks (GDN). In Section 2 a methodology is presented for the inclusion of near-source effects in the prediction of intensity measures (IM) of interest for the considered systems, while Section 3 presents an application to an example WSS. Conclusions and future work are given in Section 4.

2. Methodology

As already said, near-fault ground motions are often characterized by the rupture directivity effect in the fault-normal direction and a permanent displacement, the “fling step”, in the fault-parallel direction. Both phenomena may have strong influence on the response of elements at risk. Subsection 2.1 introduces the ground motion database employed in this work to derive a methodology, discussed in subsection 2.2, for taking into account the directivity effect for buried components. Then, a short selection of fling step models is presented in subsection 2.3.

2.1 Ground motion database

In order to develop the methodology described in subsection 2.2, 119 records from shallow crustal earthquakes occurred in active tectonic regions were extracted from the PEER (2016) ground motion database. The selected records are near-fault pulse-like ground motions characterized by forward-directivity. The two horizontal components of the ground motions were projected in the FP and the FN directions. The velocity time histories show a polarization in the FN direction and are characterized by a clear pulse in the fault-normal direction. The complete list of the earthquakes from which such ground motions were recorded is reported in Table 1, with indication of the earthquake name, year, moment magnitude M_W, number of records and range of closest distance to the rupture surface, R_{rup}. Further information about the employed records can be found in the work by Mollaioli et al. (2014).

Table 1 – Info about the near-fault pulse-like records used in this study.

Earthquake name	**Year**	M_W	**No of ground motions**	R_{rup} **<range> (km)**
Yountville	2000	5.00	1	11.50
Coyote Lake	1979	5.74	1	3.11
San Salvador	1986	5.80	2	<6.30 - 6.99>
Westmorland	1981	5.90	2	<6.50 - 16.66>
Whittier Narrows-01	1987	5.99	3	<18.49 - 24.54>
Parkfield	2004	6.00	10	<0.10 - 8.40>
N. Palm Spring	1986	6.06	2	<4.04 - 6.82>
Morgan Hill	1984	6.19	2	<3.26 - 9.86>
Chi-Chi, Taiwan-03	1999	6.20	3	<14.66 - 22.37>
Managua, Nicaragua-01	1972	6.24	1	4.06
Bam, Iran	2003	6.50	1	4.80
Imperial Valley-06	1979	6.53	13	<0.07 - 12.85>
Superstition Hills-02	1987	6.54	2	<0.95 - 18.20>
Erzican, Turkey	1992	6.69	1	4.38
Northridge-01	1994	6.69	11	<5.19 - 8.44>
Gazli, USSR	1976	6.80	1	5.46
Irpinia, Italy-01	1980	6.90	1	10.84
Kobe, Japan	1995	6.90	5	<0.27 - 3.31>
Loma Prieta	1989	6.93	5	<3.88 - 12.82>
Cape Mendocino	1992	7.01	2	<6.96 - 8.18>
Duzce, Turkey	1999	7.14	2	<6.58 - 12.04>
Landers	1992	7.28	2	<2.19 - 23.62>
Kocaeli, Turkey	1999	7.51	4	<4.83 - 15.37>
Chi-Chi, Taiwan	1999	7.62	42	<0.32 - 47.67>

2.2 Pulse extraction and amplification factor for PGV

Buried pipelines are vulnerable to Peak Ground Velocity (PGV) and Permanent Ground Deformation (PGD). In near-fault areas, the fields of both intensity measures are expected to be altered with respect to the far field. In order to take into account the alteration on PGV, a methodology was developed in this work, employing as its first step the procedure introduced by Baker (2007) to identify pulses in near-fault pulse-like records, based on a score called *pulse indicator*. Such procedure, coded in MATLAB® language and to date publicly available (Shahi and Baker, 2012), was used to identify and extract the pulse from the velocity time history of the selected pulse-like records. The extraction results are exemplified in Fig. 1, with reference to a sample record. These results have been used to establish a preliminary model of PGV amplification due to near-source effects.

After the pulse extraction, the ratio γ between the PGV of the original and the residual ground motions was computed for all records:

$$\gamma = \frac{\mathrm{PGV}}{\mathrm{PGV}_{\mathrm{resid}}} \tag{1}$$

Two possible models have been considered. A simple magnitude and distance-independent model, and a more refined one where these dependencies are accounted for. The frequency diagram in Fig. 2, left, shows that, if all amplification ratio values are processed together, irrespective of magnitude and distance, the distribution of γ is well fitted by a lognormal distribution, whose parameters, i.e. mean and standard deviation of lnγ, were determined to be 0.70 and 0.26, respectively. Using such a simple model within a simulation approach, in near-fault areas, as is the case of the example in this paper (Section 3), in each run a value for γ is randomly sampled from the lognormal distribution and used as amplification factor for PGV computed by a GMPE that neglects near-source effects.

An attempt of establishing a more refined model was also made, but was not considered further at this stage. The scatter plot of γ against M_W and $\ln R_{rup}$ (Fig. 2, right) shows the absence of correlation and highlights a rather dispersed and unexpected functional relationship between γ and the other two variables. This is confirmed by the reported root-mean-square error (RMSE), and by the inclination of the fitted plane that, in a counterintuitive way, implies that γ increases with distance from the fault. It was concluded that at this stage, using the employed records it is not possible to reliable estimate and use a magnitude- or distance-dependent γ model. Further research is needed.

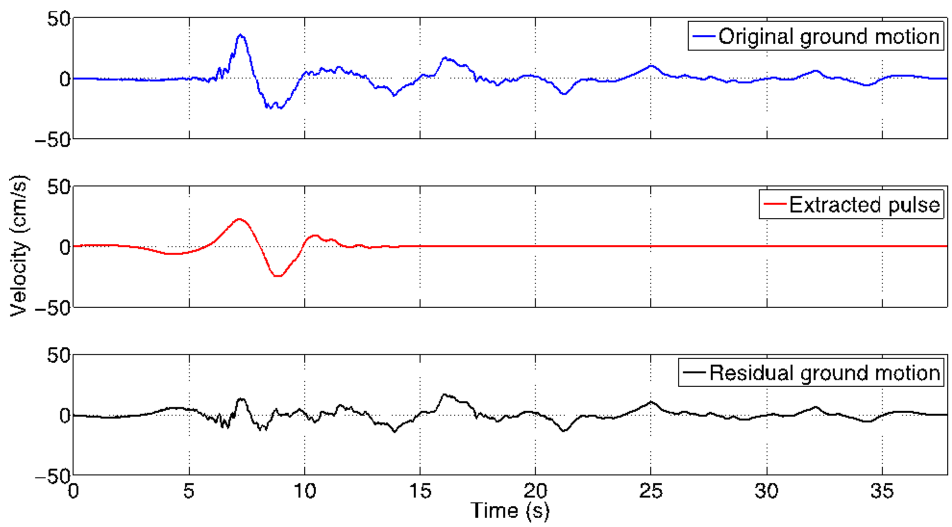

Fig. 1 – Original ground motion, extracted pulse and residual ground motion for a sample record (1979 Imperial Valley earthquake, M_W = 6.4, station of Brawley airport)

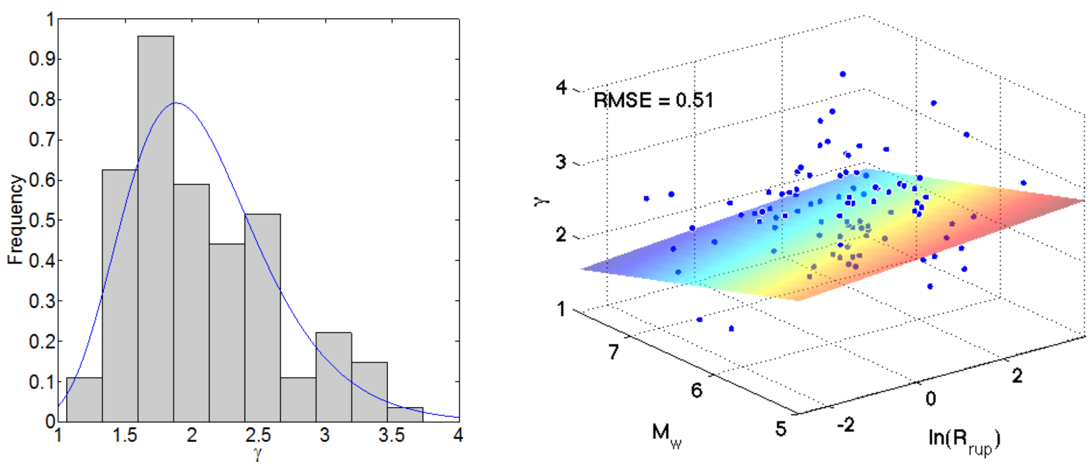

Fig. 2 – Frequency diagram of γ, with the lognormal fit superimposed (left), and scatter plot of γ against M_W and R_{rup}, with a plane fitted to data points and indication of RMSE (right)

2.3 Fling step model

During an earthquake, the two sides of the rupturing fault move relative to each another, resulting in a permanent tectonic deformation, a static ground displacement called “fling step”. This typically appears in the FP direction as a step function in the displacement time series and as a one-sided pulse in the velocity time series (recall that the forward-directivity velocity pulse is two-sided). Since the fling step pulse usually has a shorter period than the directivity pulse but occurs at about the same time, the two effects can be modeled separately and then treated as coincident events (Bray and Rodriguez-Marek, 2004; Somerville, 2002). It has to be noted that standard filtering and baseline correction procedures applied to raw ground motion records remove the static displacement, which constitutes the zero-frequency part of the seismic signal (Dabaghi and Der Kiureghian, 2014). This applies also to the database used in this work (see subsection 2.1). For this reason, instead of extracting the fling step from the records, as done for the directivity effect, in order to predict the displacement at pipe sites it was decided to adopt a fling step model available in the current literature. A short selection of fling step models available in the current literature is presented in Table 2, where D_{fault} is the mean slip over the rupture plane (D_{site} and D_{fault} are in units of centimeters), Z_{TOR} is the depth to top of rupture, L is the rupture length, W is the rupture width and α is a constant parameter equal to 0.22 (Abrahamson, 2001). All models predict the fling step at site, D_{site}: in other words, this is the displacement due to PGD, which is induced in this case by a strong earthquake striking sites located at close proximity to a fault. PGD, in general, can be caused also by other phenomena, such as liquefaction, landsliding and co-seismic rupture. Despite that in case of simultaneous occurrence such phenomena may interact with each other, usually they are treated independently and then the largest displacement due to PGD is adopted: this is also the approach followed in this framework.

Table 2 – Selection of fling step models available in the current literature

Model	Functions
Abrahamson (2001)	$\ln\left(D_{\text{fault}}\right) = 1.15 \cdot M_W - 2.83$ $D_{\text{site}} = \frac{D_{\text{fault}}}{\pi}\left(\frac{\pi}{2} - \tan^{-1}\left(\alpha \cdot R_{rup}\right)\right)$
Dreger et al. (2011)	$D_{\text{site}} = \frac{D_{\text{fault}}}{2}\left[1 - \frac{2}{\pi}\tan^{-1}\left(\frac{R_{rup}}{W}\right)\right]$ if $Z_{TOR} = 0$ $D_{\text{site}} = \frac{D_{\text{fault}}}{\pi}\left[\tan^{-1}\left(\frac{R_{rup}}{Z_{TOR}}\right) - \tan^{-1}\left(\frac{R_{rup}}{Z_{TOR} + W}\right)\right]$ if $Z_{TOR} > 0$ D_{fault} from Abrahamson (2001)
Burks and Baker (2016)	$D_{\text{site}} = \ln\left[\frac{\pi}{2} - \tan^{-1}\left(0.3 \cdot R_{rup}\right)\right] + 1.3 \cdot M_W - 5.1$
Kamai et al. (2014)	$D_{\text{fault}} = \frac{10^{1.5 \cdot M_W + 16.05}}{3 \cdot 10^{11} \cdot L \cdot W}$ L, W unknown $\Rightarrow \ln\left(D_{\text{fault}}\right) = 1.15 \cdot M_W - 3.28$ D_{site} from Abrahamson (2001)

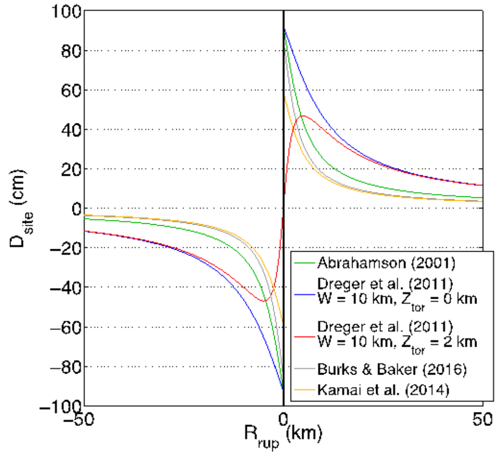

Fig. 3 – Fling step at site, D_{site}, due to a $M_W = 7$ earthquake as a function of rupture distance R_{rup}: model comparison

Fig. 3 shows the exponential decay of D_{site} with R_{rup}, according to the selected models. Given the illustrative character of this paper, for the example in Section 3 the Abrahamson (2001) model was adopted, simply because it provides approximately the mean values of D_{site} among the considered models. Since near-source records characterized by evident fling step are related to large magnitude earthquakes (see e.g. Burks and Baker, 2016), the adopted model was used in this study only for $M_W \geq 7$.

3. Example application

The methodology described in Section 2 was implemented as an extension of a civil infrastructure simulation tool, namely Object-Oriented Framework for Infrastructure Modeling and Simulation (OOFIMS) (Franchin and Cavalieri, 2010-2016), coded in MATLAB® language and recently developed in an European project (see SYNER-G, 2012).

The case-study system, shown in Fig. 4, is a water supply system characterized by grid or mesh-like topological structure, typical in urban areas of the main links connecting suburbs or districts, and can be considered as a transmission/distribution (TD) system. Dueñas-Osorio (2005) developed a network model to represent real TD systems, based on the ideal class of the *d-lattice-graph*, an unweighted, undirected, regular graph of dimension d with vertices joined to their lattice neighbors according to specified rules. First, the number of vertices n is fixed in order to obtain a square grid, since TD models exist on adjacency matrices of square topologies. Then, m edges of the complete graph (an aperiodic TD substrate) are retained with a probability of existence equal to p_m. This probability can be estimated empirically for each network typology, and the expression provided by Dueñas-Osorio (2005) for water systems is:

$$p_m = 0.60 \cdot n^{-0.05} \tag{2}$$

The total number of nodes is 36, five of which are constant-head water sources, 19 are sinks/demand nodes and the remaining ones are joints. A total of 60 cast iron pipes connect the nodes.

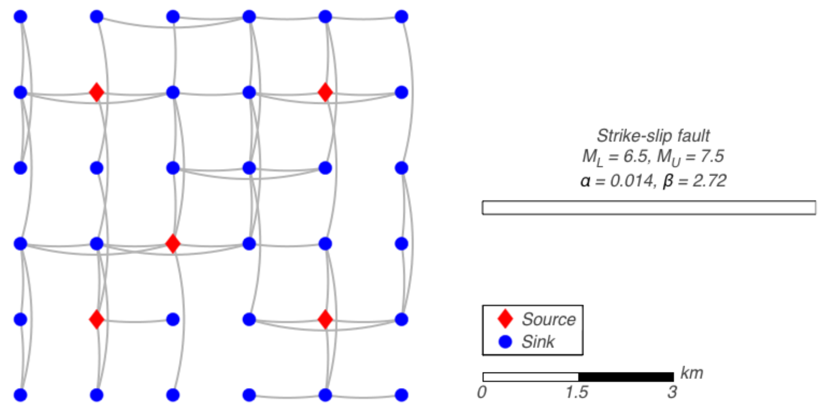

Fig. 4 – Topology of the example water supply system and seismic environment information

Only pipelines are considered to be vulnerable. In empirical models (e.g. Federal Emergency Management Agency [FEMA], 2003) the fragility of buried pipelines is usually given in terms of two Poisson repair rates per unit length, functions of PGV and PGD, respectively. The acronym PGD is here employed also to indicate the resulting displacement, which is called D_{site} in this work. Within OOFIMS, the fragility functions provided by American Lifelines Alliance (ALA, 2001) are implemented (PGV in cm/s and PGD in m):

$$\begin{aligned} \lambda_{repair}(\mathrm{PGV}) &= K_1 \cdot 0.0024 \cdot \mathrm{PGV} \\ \lambda_{repair}(\mathrm{PGD}) &= K_2 \cdot 11.224 \cdot \mathrm{PGD}^{0.319} \end{aligned} \tag{3}$$

where K_1 and K_2 are functions of the pipe material, soil, joint type and diameter and λ_{repair} is returned in km^{-1}. The number of repairs N_L for the generic pipe is randomly generated using the highest repair rate as the Poisson distribution parameter, λ. No information is provided in the fragility model about the nature of the generic repair, i.e. whether it is a leak or a break (loss of continuity due to joint pull-out or pipe separation after rupture). If $N_L > 0$, a number N_L of Bernoulli trials, θ, are conducted, with parameter p_f representing the pipe failure probability and being a function of λ: actually such probability is set to 0.2 or 0.8, depending on whether repairs are caused by PGV or PGD, respectively (ALA, 2001). If at least one Bernoulli trial gives success (i.e., a sample from a standard uniform distribution is below p_f), the pipe is considered to be broken, it is removed from the network and its leakage area $A_{leakage}$ is set equal to its cross section area, while if no breakage occurs, the total leakage area is determined as the number of leaks times the opening area of one leak. Hwang et al. (1998), on the base of empirical evidence, set the extent of such an area as 3% of the total cross section area.

The seismic environment is composed of only one strike-slip fault, whose activity parameters are indicated in Fig. 4. It should be noted that this particular artificial example is conceived so as to highlight the influence of near-source effects in the simplest possible conditions. The source model currently implemented in OOFIMS does not allow to take into account the propagation of fault rupture, but here it is assumed that rupture always propagates towards the WSS pipes, which are thus all subjected to forward-directivity. Further, the overall extension of the considered system is about 6×6 km. As such, the entire area can be thought of being subjected to an approximately uniform value of γ. By so doing the problem of estimating a distance-dependent γ model is avoided, which is convenient because, as highlighted above, the employed records (see Table 1) do not support such a model (see Fig. 2, right).

3.1 Flow model and performance metrics

The functional model for this network, as implemented in OOFIMS, consists of the $N + E$ steady-state nonlinear flow equations (Houghtalen et al., 2009):

$$\begin{cases} \mathbf{A}_D^T \mathbf{q} - \mathbf{Q}(\mathbf{h}_D) = \mathbf{0} \\ \mathbf{R}|\mathbf{q}|\mathbf{q} + (\mathbf{A}_D \mathbf{h}_D + \mathbf{A}_S \mathbf{h}_S) = \mathbf{0} \end{cases} \tag{4}$$

where N and E are the number of internal (non-source) nodes and of edges, respectively. The first N equations express flow balance at the internal nodes (sum of incoming and outgoing flows equals zero), while the next E equations express the flow resistance of the edges. The subscripts D and S denote the partitions (of vectors and matrices) referred to the N internal or demand nodes and M source nodes, respectively. The matrices $\mathbf{A}_D$ ($E \times N$) and $\mathbf{A}_S$ ($E \times M$) are sub-matrices of the $E \times (N + M)$ matrix $\mathbf{A}$, containing 0, 1 and -1 terms as a function of the network connectivity. The vectors $\mathbf{h}_D$ ($N \times 1$) and $\mathbf{h}_S$ ($M \times 1$) are the corresponding partitions of the $(N + M) \times 1$ vector $\mathbf{h}$ collecting the N unknown water heads in the internal nodes and the M known water heads in the source nodes. The $E \times 1$ vector $\mathbf{q}$ collects the unknown flows in the E edges, and $\mathbf{R}$ is the $E \times E$ diagonal matrix of resistances, with terms $r_i = u_i \cdot L_i$, where $u_i = \beta \cdot D^{-5}$ (according to Darcy's law) and L_i is the i-th edge length. The above set of equations expresses the flow analysis in "head-driven" mode, since the flows actually delivered, $\mathbf{Q}(\mathbf{h}_D)$, are reduced with respect to the end-user demands, $\mathbf{Q}$, if the (unknown) heads at internal nodes fall below thresholds $\mathbf{h}_{min}$; the latter are usually set as the average building heights in the areas served by the nodes, incremented by five meters water column. For the generic internal node this is written as:

$$Q_i(h_{D,i}) = \begin{cases} Q_i \cdot \dfrac{h_{D,i}}{h_{i,min}}, & \text{if } h_{D,i} < h_{i,min} \\ Q_i, & \text{if } h_{D,i} \geq h_{i,min} \end{cases} \tag{5}$$

This approach is preferred to the solution with fixed demands ("demand-driven" mode), especially for the perturbed seismic conditions, where satisfaction of prescribed demands is not guaranteed (it's an assessment rather than a design problem).

Among the performance metrics implemented in OOFIMS, two system-level metrics for WSS are of interest in this work. They are flow-based, involving the computation of flows and heads in the network: as such, they automatically take into account the network connectivity. The first metric is the Average Head Ratio (AHR), defined in Franchin et al. (2013) as the average over the internal nodes of the head ratio (HR), which in turn is the ratio of the water head in seismically damaged network over the reference value for the non-seismic, normal operation conditions ($h_{D,i0}$):

$$\mathrm{AHR} = \frac{1}{N}\sum_{i=1}^{N} HR_i = \frac{1}{N}\sum_{i=1}^{N} \frac{h_{D,i}}{h_{D,i0}} \tag{6}$$

The second metric is the System Serviceability Index (SSI), introduced by Wang et al. (2010):

$$\mathrm{SSI} = 100\frac{\sum_{i=1}^{N} Q_i(h_{D,i})}{\sum_{i=1}^{N} Q_i} \tag{7}$$

where $Q_i(h_{D,i})$ and Q_i have been defined above and are referred to the damaged and undamaged conditions, respectively. The SSI index varies between 0 and 100, assuming the value 0 when there is no solution for the flow analysis (i.e., AHR = 0) and 100 when the WSS remains undamaged after the earthquake, or the water head at all sink nodes is larger than the threshold.

3.2 Results

The performance assessment of a lifeline in a seismically active area presents several input uncertainties, in the regional seismicity and the fragility of network components. In order to take into account such uncertainties and highlight the impact of near-source effects (directivity plus fling step), two Monte Carlo simulations with 1000 runs each were carried out, in which the near-source effects were neglected or considered, respectively. It has to be noted that all the random variables were assigned the same sets of values in the two simulations, to capture the exclusive influence of near-source effects modeling on the performance assessment of the example WSS.

The alterations of intensity measures related to transient and permanent ground deformation are shown in Fig. 5, left, with reference to two sample seismic scenarios within the Monte Carlo simulation with near-source consideration. In particular, Fig. 5 shows a shake map in terms of PGV, as obtained with the Akkar and Bommer (2010) GMPE, including the spatial correlation between the intra-event residuals; the PGV values are amplified by the factor $\gamma = 2.29$, sampled from its lognormal distribution. On the other hand, Fig. 5, right, shows the field of permanent ground deformation, D_{site}, which notwithstanding the exponential decrease, still reaches non-negligible values everywhere in the area of interest for the considered event. It is assumed that the area of interest is not susceptible to liquefaction and landsliding and hence would not experience permanent ground deformation if near-source effects were neglected.

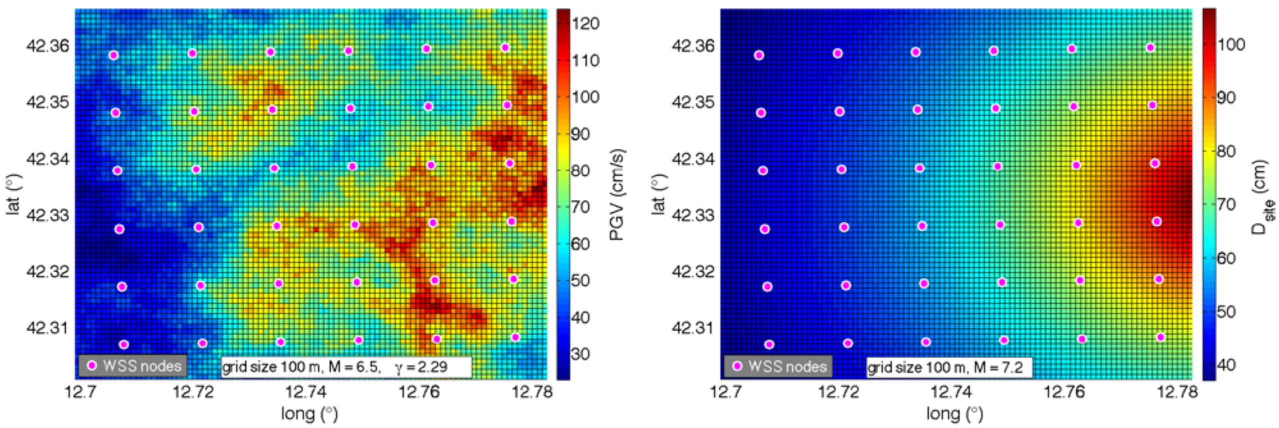

Fig. 5 – Sample Monte Carlo simulation runs: PGV field (left) and D_{site} field (right)

Fig. 6 shows the moving average μ of the two considered performance metrics, together with the curves of μ plus and minus the moving standard deviation σ, with and without near-source effects (directivity plus fling step).

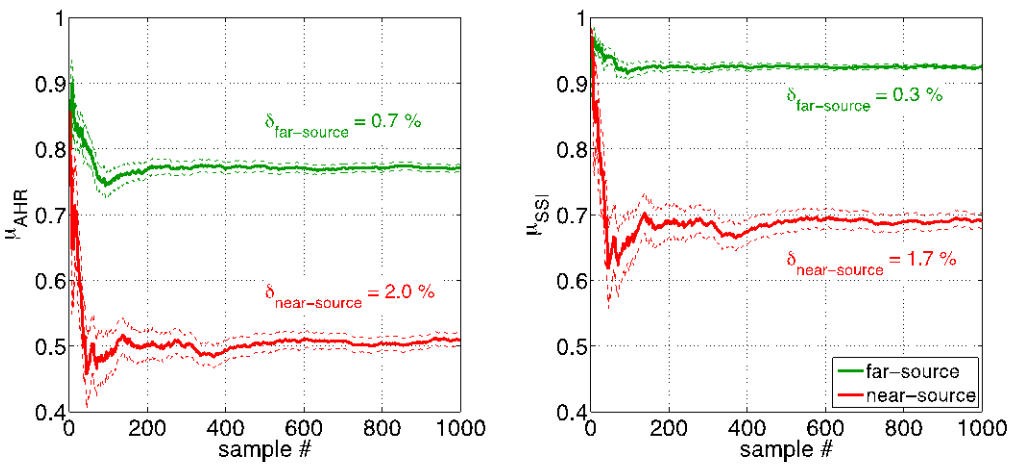

Fig. 6 – Moving average with indication of moving standard deviation, for AHR (left) and SSI (right), with and without the near-source effects (directivity plus fling step)

As expected, when such effects are considered the mean of both metrics decreases and the standard deviation increases, leading to the increase of variability and hence of the coefficient of variation $\delta = \sigma / \mu$. The figure indicates that the adopted number of runs is sufficient to stabilize the estimates of both metrics in both conditions, but it is clear that in general in the presence of near-source effects a longer simulation is needed to stabilize μ and reduce δ. The percent reduction of μ, as well as the increment of δ, are similar for the two metrics, while the difference between them can be seen in the fact that SSI presents a lower variability in both the "far-source" and the "near-source" cases, compared to AHR. It can be concluded from this figure that AHR and SSI for the case-study network are impacted in a similar way by the near-source effects.

The frequency diagrams of AHR and SSI, resulting from the two Monte Carlo simulations, are shown in Fig. 7, with and without near-source effects. It can be noted that for both metrics the impact of PGV amplification and fling step on the extreme values (0, 1) is much larger than on intermediate values. This is an important concern for an asset located in proximity of an active fault, since an increased probability (obtained multiplying the frequency by the discretization step) of attaining the minimum value of such parameters may indicate a higher probability of total disruption, depending on the properties of the infrastructure at hand, such as the availability of backup power for pumping stations and the height of buildings to be fed with potable water. For the considered example, the heavy damage induced by near-source effects, especially by fling step, leads to high probability to experience null AHR, triggering a dramatic decrease of functionality (null SSI).

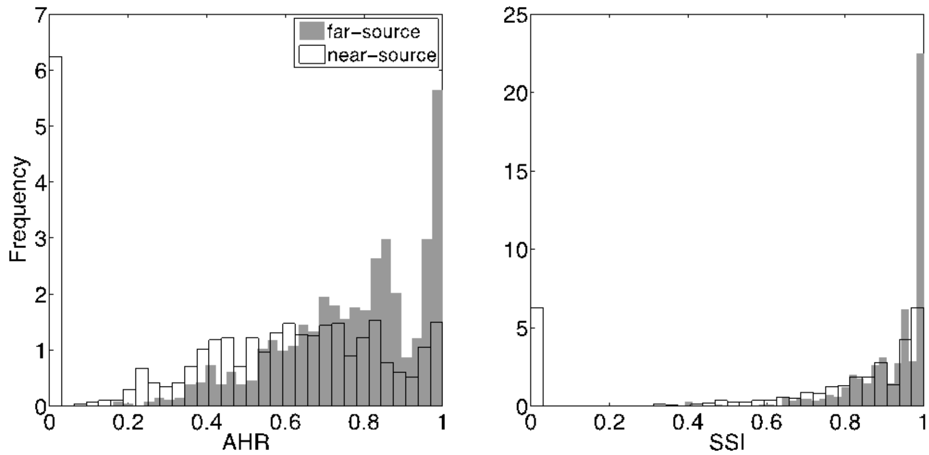

Fig. 7 – Frequency diagrams of AHR (left) and SSI (right), with and without the near-source effects

Fig. 8 shows the cumulative distribution functions (CDF) of AHR and SSI, for both cases. It is clear from the graphs how the probability that the metrics take values lower than or equal to a generic value increases up to 20% for lower values, i.e. the ones with the greatest impact on the performance. In order to get a measure of the distance between the CDFs in the two cases, it is possible to evaluate the probability distribution P of both metrics obtained from the two simulations and to compare them formally through a distribution matching metric like the Kullback–Leibler divergence, written here for AHR:

$$D_{KL}\left(P_{AHR,NS} \,\|\, P_{AHR,FS}\right) = \sum_{i=1}^{1000} P_{AHR,NS}\left(AHR_i\right) \ln \frac{P_{AHR,NS}\left(AHR_i\right)}{P_{AHR,FS}\left(AHR_i\right)} \tag{8}$$

where NS and FS stand for "near-source" and "far-source", respectively. Analogously, Eq. (8) can be related to SSI. D_{KL} is written here in its discrete form since the distributions are the experimental ones obtained from the simulations. The higher D_{KL} value reached for AHR reflects what is shown in Fig. 7 in terms of frequency diagrams, i.e. the larger distance between the two distributions for intermediate values. This is justified by the fact that AHR receives a direct impact from pipeline damage, while SSI, being related to delivered flow, is a consequence of head loss and also depends on thresholds $\mathbf{h}_{min}$.

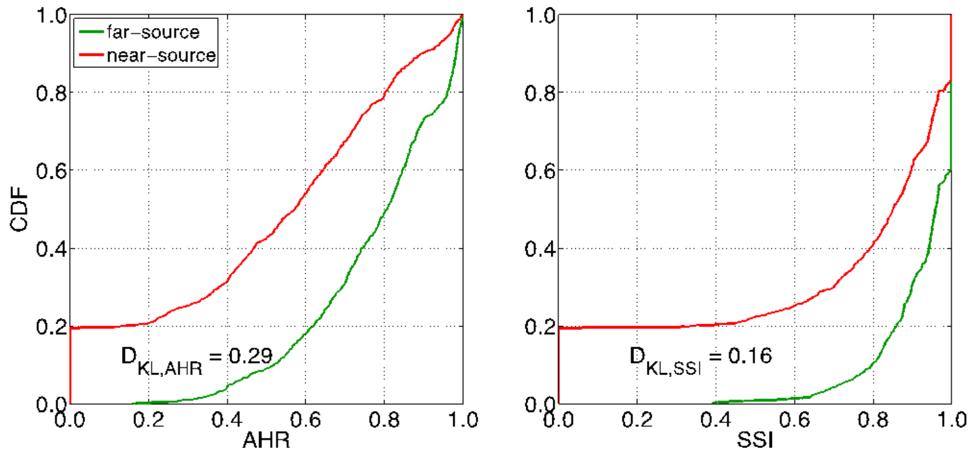

Fig. 8 – CDF of AHR (left) and SSI (right), with and without the near-source effects, and indication of the Kullback–Leibler divergence for the two metrics

4. Conclusions and future work

The paper presents a preliminary investigation of the influence of near-source effects, included in the prediction of PGV and PGD, on the performance of spatially distributed systems composed of buried pipelines, such as water or gas distributions networks. The methodology was implemented as an extension of OOFIMS, a recently developed simulation framework for vulnerability and risk assessment of civil infrastructures. An example application of probabilistic performance assessment, via Monte Carlo simulation, of a small water supply system in a near-fault area was carried out. Two simulations were considered, with and without near-source effects. The results, presented in terms of the predicted fields of transient (PGV) and permanent (PGD) ground deformation, as well as of the probability distributions of two flow-based system-level performance metrics, showed that the consideration of directivity effects and fling step may lead to non-negligible alterations of seismic IM fields and, as a consequence, of system performance. Future work aims to enhance the inclusion of near-fault effects in the spatial hazard model by: i) introducing more near-source pulse-like ground motion records in the database; ii) investigate the dependence on distance (and possibly magnitude and azimuth) of near-source amplification factors; iii) modifying the spatial correlation model for intra-event residuals, taking into account near-source effects, in existing ground motion prediction equations for “classical” IMs ($S_a(T)$, PGA, PGV); iii) extend the methodology to other IMs that may impact the infrastructural systems, such as the energy-based ones (e.g., energy equivalent velocity V_{EI}).

5. Acknowledgements

This work was supported by the Italian Ministry of the Instruction, University and Research (MIUR) under the research program of Sapienza University of Rome (project grant number C26A14Z7WX) and in part by DPC-Reluis 2014–2016. This support is gratefully acknowledged. Any opinions, findings, and conclusions or recommendations expressed in this material are those of the authors and do not necessarily reflect those of the sponsor.

6. References

[1] Abrahamson, NA (2001): Development of fling model for Diablo Canyon ISFSI, Pacific Gas and Electric Company. Geosciences Department, Calc. No. GEO. DCPP, 1.

[2] Akkar, S, Bommer, JJ (2010): Empirical equations for the prediction of PGA, PGV and spectral accelerations in Europe, the Mediterranean region and the Middle East. *Seismological Research Letters*, **81**(2), 195-206.

[3] American Lifeline Alliance (ALA) (2001): Seismic fragility formulation for water systems. Part 1 - guideline (ASCE-FEMA). G&E Engineering Systems Inc., 6315 Swainland Rd, Oakland, CA 94611, USA.

[4] Baker, JW (2007): Quantitative classification of near-fault ground motions using wavelet analysis. *Bulletin of the Seismological Society of America*. **97**(5), 1486-1501.

[5] Bray, JD, Rodriguez-Marek, A (2004): Characterization of forward-directivity ground motions in the near-fault region, *Soil Dyn. Earthq. Eng.*, **24**(11), 815-828.

[6] Burks, LS, Baker, JW (2016): A predictive model for fling-step in near-fault ground motions based on recordings and simulations. *Soil Dynamics and Earthquake Engineering*, **80**, 119-126.

[7] Dabaghi, M, Der Kiureghian, A (2014): Stochastic Modeling and Simulation of Near-Fault Ground Motions for Performance-Based Earthquake Engineering. PEER Report 2014/20.

[8] Dreger, D, Hurtado, G, Chopra, A, Larsen, S (2011): Near-field across-fault seismic ground motions. *Bulletin of the Seismological Society of America*, **101**(1), 202-221.

[9] Dueñas-Osorio, L (2005): Interdependent response of networked systems to natural hazards and intentional disruptions. Ph.D. thesis, Georgia Institute of Technology.

[10] Federal Emergency Management Agency (FEMA) (2003): Multi-hazard loss estimation methodology: Earthquake Model: HAZUS®MH MR4, technical manual. Department of Homeland Security Emergency Preparedness and Response Directorate, Federal Emergency Management Agency, USA.

[11] Franchin, P, Taucer, F, Hancilar, U (Eds) (2013): Methodology for Systemic Seismic Vulnerability Assessment of Buildings, Infrastructures, Networks and Socio-Economic Impacts. SYNER-G Reference Report 1. Luxembourg: Publications Office of the European Union.

[12] Franchin, P, Cavalieri, F (2010-2016): OOFIMS (Object-Oriented Framework for Infrastructure Modeling and Simulation). Available: https://sites.google.com/a/uniroma1.it/oofims/ [2016, May 10].

[13] Houghtalen, RJ, Akan, AO, Hwang, NHC (2009): Fundamentals of Hydraulic Engineering Systems (4th edition). Prentice Hall, Boston, MA.

[14] Hwang H, Lin H, Shinozuka M (1998): Seismic Performance Assessment of Water Delivery Systems. *Journal of Infrastructure Systems*, **4**(3), 118-125.

[15] Kamai, R, Abrahamson, N, Graves, R (2014): Adding fling effects to processed ground-motion time histories. *Bulletin of the Seismological Society of America*, **104**(4), 1914-1929.

[16] Mollaioli, F, Liberatore, L, Lucchini, A (2014): Displacement damping modification factors for pulse-like and ordinary records. *Engineering Structures*, **78**, 17-27.

[17] Pacific Earthquake Engineering Research Center (PEER) (2016): Ground Motion Database. Available: http://ngawest2.berkeley.edu/ [2016, May 10].

[18] PCCIP (1997): Critical foundations: Protecting America's Infrastructures. Report of the President's Commission on Critical Infrastructure Protection, Available: http://www.fas.org/sgp/library/pccip.pdf [2016, May 10].

[19] Rinaldi, SM (2004): Modeling and simulating critical infrastructures and their interdependencies. *Proceedings, Thirty-Seventh Annual Hawaii International Conference on System Sciences*, Big Island, HI, USA.

[20] Shahi, SK, Baker, JW (2012): software tool in MATLAB® language. Available: http://web.stanford.edu/~bakerjw/pulse-classification.html [2016, May 10].

[21] Somerville, PG, Smith, NF, Graves, RW, Abrahamson, NA (1997): Modification of Empirical Strong Ground Motion Attenuation Relations to Include the Amplitude and Duration Effects of Rupture Directivity, *Seism. Res. Letters*, **68**(1), 199-222.

[22] Somerville, PG (2002): Characterizing near fault ground motion for the design and evaluation of bridges. *Proceedings, 3rd National Conference & Workshop on Bridges and Highways*, Portland, OR, USA.

[23] SYNER-G (2012): Collaborative Research Project, funded by the European Union within Framework Programme 7 (2007–2013), under Grant Agreement no. 244061. Available: http://www.syner-g.eu/ [2016, May 10].

[24] Wang Y, Siu-Kui A, Qiang F (2010): Seismic Risk Assessment and Mitigation of Water Supply Systems. *Earthquake Spectra*, **26**(1), 257-274.